Three-Dimensional Integral Method for Modeling Electromagnetic Inductive Processes

Annie Gagnoud

***Abstract*—This paper describes a three-dimensional integral method that models electromagnetic phenomena taking place during inductive melting. The method is well suited to inductive systems undergoing sinusoidal excitation at midrange or high frequencies. Under these conditions, only the surfaces of the conductors need to be meshed. The unknowns of the model are current density and scalar electrical potential. Power density, electromagnetic forces, and electrical impedance can easily be derived. Comparisons between numerical results and measurements confirm the accuracy of the model.**

***Index Terms*—Eddy currents, induction heating, integral equations, numerical analysis.**

I. Introduction

IN INDUCTION melting, a sinusoidal variation of the exciting current creates eddy currents in the material to be melted. The frequency of the excitation signal is generally in the kilohertz range. An induction-melting installation mainly consists of an inductor coil surrounding a crucible that contains the load. Different kinds of crucibles exist for different applications. The crucible may be cylindrical, segmented, or have a rectangular cross section, and can be made of electrically conducting or nonconducting materials. The load can be an insulator, such as an oxide, a semiconductor, or an electrical conductor. For computational reasons, configurations are often assumed to be axisymmetric. However, for certain shapes, for example, those used in continuous casting or cold crucible processes, better results can be obtained by taking into account the three-dimensional (3-D) nature of the configuration.

In induction-melting installations, conductors and nonmagnetic materials are exposed to relatively high frequencies (>kHz). This can cause difficulties in numerical modeling due to the small skin depth. Further complications are introduced by the 3-D geometry, the small slit width separating segments (for cold crucible devices), and the infinite boundary conditions.

Different numerical approaches have been used to model this kind of electromagnetic problem, including the finite-element, boundary-integral, moment, and integral methods.

The finite-element method has long been used to solve 3-D eddy-current problems involving a variety of unknowns and formulations. The stability and accuracy vary according to the solution chosen. Various 3-D magnetic vector potential formulations have been developed, studied, and compared [1]. Many authors concentrated on the conditions ensuring the uniqueness of the potentials and the stability of the finite-element formulations at low and high frequencies. A number of authors have adopted formulations using the magnetic vector potential $\overrightarrow{A}$ and the electrical potential V to solve 3-D eddy-current problems. This 3-D approach can be used to determine the shape of the free surface in cold crucible systems and to study the influence of the frequency on the shape of the molten surface in a rectangular cold crucible [2]. A formulation using magnetic vector potential $\overrightarrow{A}$ and electrical vector potential $\overrightarrow{T}$ has been applied with the edge-element technique [3]. This approach is of interest for magnetic regions with different permeabilities. The authors compared this formulation with the classical method and discussed its advantages. This method was applied to induction heating systems.

With all numerical methods, it is difficult to take into account the consequences of a thin-skin effect and unbounded domain. Different ways of dealing with the small skin depth have been proposed.

A current sheet approximation can be used to model the weak penetration of the eddy current in an integro-differential method to model the cold crucible device [4], [5].

Another solution is to use the surface boundary impedance, based on a one-dimensional (1-D) approximation, combined with the replacement of the conductors by a boundary condition. The impedance boundary condition is an effective method that can handle skin depth effects in linear media. This condition is used in both the finite-element and boundary-integral methods. A number of articles have been published on this subject.

The use of this boundary condition and the errors that can occur when the approximation is not justified have been previously discussed [6]. A modified surface impedance for an edge in the transverse electric case has been proposed and compared with the classical impedance. Elsewhere, a high-order surface impedance boundary condition (SIBC) has been combined with the finite-element method [7]. This high-order SIBC presents some advantages including higher accuracy and the possibility of taking the effects of the curvature of the conductor surface into account. A methodology to select the order of approximation best suited to a given problem has been proposed [8]. A 3-D finite-element model coupled with impedance boundary conditions has also been developed and applied to the study of radio-frequency plasma [9]. We have previously proposed a 3-D finite-element formulation $\overrightarrow{A}, V$ with an impedance boundary condition to study electromagnetic continuous casting. The free surface of the meniscus is determined by the pressure equilibrium [10].

The boundary-integral method is also currently used to model 3-D eddy currents. A boundary-integral formulation, with simple single and dual layers, is well adapted to large and complex applications because the number of unknowns is

Manuscript received September 18, 2002; revised October 2, 2003.

The author is with the CNRS EPM Laboratory, 38402 Saint Martin d'Hères, France (e-mail: gagnoud@grenoble.cnrs.fr).

Digital Object Identifier 10.1109/TMAG.2003.821117

reduced to a minimum [11]. An original 3-D method has been proposed to extend the application of the surface impedance to nonlinear materials and applied to the induction hardening process [12].

The integral or moment method can also be used to solve the thin-skin eddy-current problem for a linear material. In the past, this method has generally been applied to axisymmetric geometries [13].

We have extended this model to the cylindrical cold crucible configuration and proposed a method to take the segmentation of the cold crucible into account [14].

Our aim is to develop a 3-D numerical model that is capable of describing electromagnetic problems including skin effects in linear materials. It is important to know global quantities such as joule power, electrical impedance, and local values of parameters such as power density and electromagnetic forces. Local parameters can be determined by classical methods (finite elements or boundary integral). However, it is rather difficult to obtain values for global quantities, such as electrical impedance, and to choose a stable formulation for the 3-D problem. The integral method uses the current density $\overrightarrow{J}$ and the electrical potential V; it is based on the local Ohm's law, the Biot–Savart relationship, and the conservation of current. Only the active electrical part of the domain is meshed. These physical relationships are used directly in the numerical formulation, which leads to a linear system. It is possible to calculate the local values for power density and force density as well as global values such as joule power and electrical impedance. The electrical impedance can be directly deduced from the solution. The difficulty lies in extending this methodology to 3-D geometry. For this reason, it is important to develop a general numerical approach.

In three dimensions, this method is of particular interest when the electromagnetic skin depth is small compared to the size of the conductors: the mesh is limited to the surface and, consequently, the range of the linear system is reduced.

II. 3-D Integral Method

The objective here is to implement a new numerical method, based on a physical approach and adapted to inductive melting processes and the modeling of 3-D configurations. To obtain a general approach, we use the interpolation, derivation, and integration techniques commonly used in the finite-element method. In this way, it is possible to adapt the integral method or moment method (MM) to complex 3-D geometries.

A. Physical Equations

The two equations on which the model is based are:

- the local Ohm's law equation

$$\overrightarrow{J} = -\sigma \overrightarrow{\nabla}(V) - \sigma \frac{\partial \overrightarrow{A}}{\partial t} \tag{1}$$

  where $\overrightarrow{J}$ is the current density, σ is the electrical conductivity, V is the electrical scalar potential, $\overrightarrow{A}$ is the magnetic vector potential, and t is time;
- and the equation for the conservation of current

$$\operatorname{div} \overrightarrow{J} = 0. \tag{2}$$

In the conditions of interest here, it is possible to use a particular solution of the vector potential. In an inductive melting process, the interaction between the velocity of the melt and the magnetic field can be neglected. The local expression of the potential vector is obtained by the Biot–Savart law

$$\overrightarrow{A} = \iiint_{\Omega} \frac{\mu_0 \overrightarrow{J}}{(4\pi r)} dv \tag{3}$$

Ω represents the volume of the conductors, μ_0 the magnetic permeability of air, while r represents the distance between the point concerned (point where the potential is calculated) and the source point in the volume Ω. This relationship implicitly takes into account the boundary condition at infinity.

Given the alternating nature of the exciting current, complex notation is required to express the electromagnetic quantities. Relation (1) becomes

$$\overrightarrow{J_c} = -\sigma \overrightarrow{\nabla}(V_c) - i_c \sigma \omega \overrightarrow{A_c}. \tag{4}$$

The subscript c denotes the complex value of the variable, ω is the angular frequency, and $i_c = \sqrt{-1}$.

When the Biot–Savart law (3) is substituted in the Ohm's law (4), we obtain an integral relationship between the current density and the electrical potential

$$\overrightarrow{J_c} = -\sigma \overrightarrow{\nabla}(V_c) - i_c \sigma \omega \iiint_{\Omega} \frac{\mu_0 \overrightarrow{J_c}}{(4\pi r)} dv. \tag{5}$$

Our electromagnetic problem can then be described by (2) and (5). These relations only apply to the conducting regions. Note that with this approach, the current density and electrical potential become the unknowns.

The electromagnetic skin depth is defined by $\delta = \sqrt{(2/\mu_0 \sigma \omega)}$. When the frequency is around 10 kHz and the load is an electrical conductor ($\sigma > 10^6\ \Omega^{-1} \cdot \mathrm{m}^{-1}$), the skin depth ($\delta < 5 \times 10^{-3}$ m) is very small compared to the size of the device (0.05 m to 1 m). It is, therefore, possible to apply an exponential decay when the 1-D approximation is valid

$$\overrightarrow{J_c} = \overrightarrow{J_{c,s}} e^{-\frac{(1+i_c)n}{\delta}} \tag{6}$$

where $\overrightarrow{J_{c,s}}$ is the complex value of the current density at the surface of the conductor, and n is the distance of an internal point to the surface in the direction normal to the surface. The decay law (6) is substituted in the integral in relationship (5).

When the electrical conductivity has small variations, the integral on each conductor can be separated into the product of two integrals: one with respect to the normal at the surface of the conductor and the other with respect to the surface of conductor Γ. The integral, therefore, becomes

$$\iiint_{\Omega} \frac{\mu_0 \overrightarrow{J_c}}{(4\pi r)} dv = \iint_{\Gamma} \left(\frac{\mu_0}{4\pi r} \overrightarrow{J_{c,s}} ds \right) \cdot \int e^{-\frac{(1+i_c)n}{\delta}} dn. \tag{7}$$

Relationship (7), based on the impedance boundary condition (IBC), is valid when the radius of curvature is significant and the surface point is far from the edges and corners. Therefore, when

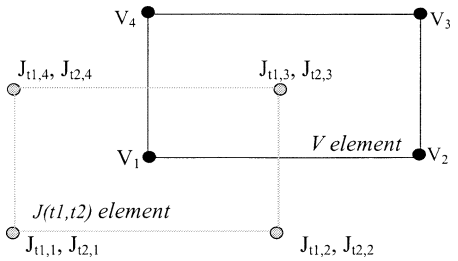

Fig. 1. First-order staggered elements on a plane surface. The current density has two components on the vectors tangent to the surface $t1$, $t2$.

the surface of the conductor has edges and corners, relationship (7) is not accurate and the resulting error depends on the configuration of the electric field and skin depth [6]. We have not yet introduced an adjustment to the boundary impedance condition. In a future publication, we will examine the possibility of introducing a better-adapted model.

Consequently, for thin-skin conditions, knowledge of the current density and electrical potential at the surface of the conductor is sufficient to describe the current density everywhere in the conductor.

B. Mesh of the Studied Domain

Generally, the various components of an inductive melting installation are relatively simple. The conductors can be described by elementary volumes such as hexahedrons, cylinders, cones, and helixes. The liquid surface is smooth and its shape results from an equilibrium between magnetic pressure, hydrostatic pressure, and surface tension. For example, the liquid surface can have a meniscus shape, as in continuous casting of steel or in a cold crucible.

In this approach, only the conductors are meshed. The geometry is, therefore, a set of objects. Simple shapes such as hexahedrons or cylinders are considered; more complex shapes will be studied in the future.

The unknowns are the current density $\overrightarrow{J}$ and electrical potential V. The current density vector is tangent to the surface of the conductor, because $\overrightarrow{J}$ is only defined in the conductor, skin depth is thin, and $\mathrm{div}(\overrightarrow{J}) = 0$. Therefore, the problem can be described using only three complex unknowns corresponding to the two components of the current density plus the electrical scalar potential. The skin is thin and, therefore, the mesh is limited to the surface of the conducting region. Two staggered meshes are used, one for the scalar potential and the other for the current density. The nodes of the current density are the center of the scalar potential elements.

The algorithm for the mesh is based on five steps.

- Creation of V nodes on the surface of each object.
- Creation of the V elements of each object.
- Creation of $\overrightarrow{J}$ nodes, for which the coordinates are calculated at the center of V elements by polynomial interpolation. The two tangential vectors are calculated by derivation (Fig. 1).
- Creation of nodes $\overrightarrow{J}$ on the edges of the objects.
- Creation of the $\overrightarrow{J}$ elements.

Fig. 2 shows an example of a mesh for a hexahedron. When the object is not smooth, difficulties arise in dealing with the current density at edges and corners. These difficulties are related to the

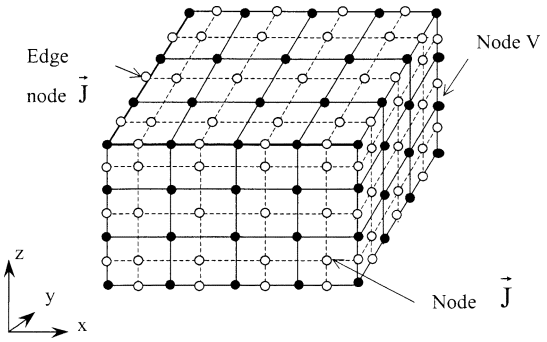

Fig. 2. Example of a mesh of the surface of a hexahedron with first-order elements. Quadrilateral V elements are represented by solid lines and quadrilateral $\overrightarrow{J}$ elements by broken lines.

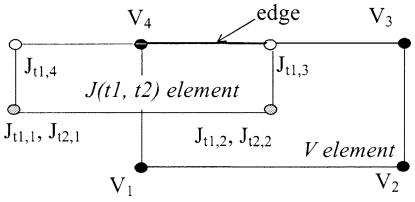

Fig. 3. First-order staggered elements near an edge. The current density nodes 3 and 4 have one component along the vector $t1$ tangent to the edge.

choice of both the decay law and the unknowns. The density is zero on corners and has a tangential orientation on the edges. Care must be taken when creating the density elements in the vicinity of edges (Fig. 3) and corners.

C. Numerical Implementation

It has been previously shown that the quantities $\overrightarrow{J}$ and V may be calculated by solving the two relationships (2) and (5) at the surface of the conducting regions.

1) Ohm's Law: Ohm's law (5) is written at each current density node i of the mesh. In this relationship, two terms have to be expressed with respect to the unknowns at the nodes: the gradient of the electrical potential and the integral. Polynomial interpolation is used to calculate the gradient and integral.

On each V element, the electrical potential is interpolated using the first-order Lagrange polynomial with NBN nodes

$$V_c = \sum_{l=1}^{NBN} \alpha_{V,l}(x,y,z) V_{c,l} \tag{8}$$

where $V_{c,l}$ is the complex value of the electrical scalar potential at node l, and $\alpha_{V,l}(x,y,z)$ is the polynomial interpolation function l on the V element. Using this interpolation, components of the gradient of the scalar potential can be expressed by the derivative of the polynomial function with respect to the coordinates of the reference element as follows:

$$\begin{aligned}
\frac{\partial V_c}{\partial x} &= \sum_{l=1}^{NBN} \left[\frac{\partial \alpha_l(\xi,\eta)}{\partial \xi} \cdot \frac{\partial \xi}{\partial x} + \frac{\partial \alpha_l(\xi,\eta)}{\partial \eta} \cdot \frac{\partial \eta}{\partial x} \right] V_{c,l} \\
\frac{\partial V_c}{\partial y} &= \sum_{l=1}^{NBN} \left[\frac{\partial \alpha_l(\xi,\eta)}{\partial \xi} \cdot \frac{\partial \xi}{\partial y} + \frac{\partial \alpha_l(\xi,\eta)}{\partial \eta} \cdot \frac{\partial \eta}{\partial y} \right] V_{c,l} \\
\frac{\partial V_c}{\partial z} &= \sum_{l=1}^{NBN} \left[\frac{\partial \alpha_l(\xi,\eta)}{\partial \xi} \cdot \frac{\partial \xi}{\partial z} + \frac{\partial \alpha_l(\xi,\eta)}{\partial \eta} \cdot \frac{\partial \eta}{\partial z} \right] V_{c,l}.
\end{aligned} \tag{9}$$

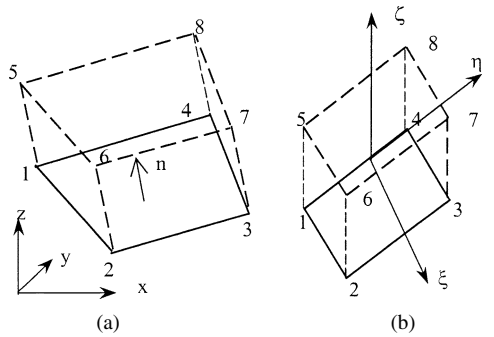

Fig. 4. Example of a 3-D element (cube) associated with a quadrilateral element (square). (a) Real 3-D element. (b) Cube.

We write $\alpha_l(\xi,\eta)=\alpha_{V,l}(x,y,z)$.

The gradient of V is calculated at the current density node i at the center of the electrical potential element, i.e., at the coordinates ($\xi=0$, $\eta=0$) of the reference element V. The mesh is constituted by surface elements in a 3-D configuration. To obtain a general approach, a 3-D element is constructed on the surface element V by adding the normal vector $\overrightarrow{n}$ of the surface element to each node (Fig. 4). The Jacobian matrix is calculated for this 3-D element. In this way, it is possible to calculate the value of the gradient at the current density node i with coordinates ($\xi=0$, $\eta=0$, $\zeta=-1$) in the 3-D reference element associated with the electrical potential surface element.

When the inductor coil is not modeled, the current density is imposed in the coil. Therefore, the integral is the sum of two integrals

$$\iiint_{\Omega}\frac{\mu_0\overrightarrow{J_c}}{4\pi r}dv=\iiint_{\Omega_{\rm Ed}}\frac{\mu_0\overrightarrow{J_c}}{4\pi r}dv+\iiint_{\Omega_{\rm Coil}}\frac{\mu_0\overrightarrow{J_{\rm coil}}}{4\pi r}dv$$

$\Omega_{\rm Coil}$ is the inductor coil domain and $\Omega_{\rm Ed}$ is the domain occupied by the conductors with eddy currents. Hence relationship (7) is applied to calculate the integral with respect to the conductors with thin-skin eddy currents. It is possible to express the integral on the surfaces of eddy-current conductors as a sum of the integrals of each surface element of the current density mesh.

The integral on the eddy-current conductors now becomes

$$\iiint_{\Omega_{\rm Ed}}\frac{\mu_0\overrightarrow{J_c}}{4\pi r}dv=\sum_{e=1}^{NEJ}\left[\iint_{S_e}\frac{\mu_0\overrightarrow{J_{c,s}}}{4\pi r}ds\cdot\int e^{-\frac{(1+i_c)n}{\delta_e}}dn\right] \tag{10}$$

where NEJ is the total number of surface elements of the current density mesh, S_e the surface area of the current density element e and δ_e the skin depth in element e. The following relationship analytically calculates the integral with respect to the normal direction for a small skin depth:

$$\int e^{-\frac{(1+i_c)n}{\delta_e}}dn\cong\int_0^{\infty}e^{-\frac{(1+i_c)n}{\delta_e}}dn=\frac{\delta_e}{(1+i_c)}.$$

A Lagrange polynomial interpolation is used to express the value of the complex current density at the surface of the conductor

$$\overrightarrow{J_{c,s}}=\sum_{j=1}^{NBN}\alpha_{J,j}(x,y,z)\overrightarrow{J_{c,s,j}} \tag{11}$$

NBN represents the number of the nodes of element J and $\alpha_{J,j}$ is the polynomial interpolation function j on the current density element. The following relation may thus be obtained:

$$\iiint_{\Omega_{Ed}}\frac{\mu_0\overrightarrow{J_c}}{4\pi r}dv=\frac{\mu_0}{4\pi}\cdot\frac{1-i_c}{2}\cdot\sum_{e=1}^{NEJ}\delta_e\left[\iint_{Se}\sum_{j=1}^{NBN}\frac{\alpha_{J,j}(x,y,z)}{r}\cdot\overrightarrow{J_{s,c,j}}ds\right]. \tag{12}$$

The real coordinates of a point (x,y,z) of an element e can be expressed by the Lagrange functions $\alpha_k(\xi,\eta)$ of the reference elements as follows for example for x coordinates:

$$x=\sum_{k=1}^{NBN}\alpha_k(\xi,\eta)x_{J,k} \tag{13}$$

where $x_{J,k}$ represents the first coordinate of node k of the element. Actually, the geometrical functions are the same functions used for the interpolation of the unknowns. The differential of area ds can be expressed by vectors $\overrightarrow{A_1}$ and $\overrightarrow{A_2}$ by the relation

$$ds=|\overrightarrow{A_1}\wedge\overrightarrow{A_2}|d\xi d\eta \tag{14}$$

$$[\overrightarrow{A_1}]=\begin{bmatrix}\sum_{k=1}^{NBN}\frac{\partial\alpha_k}{\partial\xi}x_{J,k}\\ \sum_{k=1}^{NBN}\frac{\partial\alpha_k}{\partial\xi}y_{J,k}\\ \sum_{k=1}^{NBN}\frac{\partial\alpha_k}{\partial\xi}z_{J,k}\end{bmatrix}$$

$$[\overrightarrow{A_2}]=\begin{bmatrix}\sum_{k=1}^{NBN}\frac{\partial\alpha_k}{\partial\eta}x_{J,k}\\ \sum_{k=1}^{NBN}\frac{\partial\alpha_k}{\partial\eta}y_{J,k}\\ \sum_{k=1}^{NBN}\frac{\partial\alpha_k}{\partial\eta}z_{J,k}\end{bmatrix}. \tag{15}$$

The density at node j is extracted from the integral with respect to the surface S_e. To calculate the integral, we use numerical methods: the Gauss method for a quadrilateral element and the Hammer method for a triangular element.

Ohm's law at each node i of the current density mesh is given by the following relation:

$$\overrightarrow{J_{s,c,i}}=-\sigma_i\overrightarrow{\rm grad_i}(V_c)-\frac{i_c\mu_0\omega\sigma_i}{4\pi}\overrightarrow{J_{\rm coil}}\iiint_{\Omega_{\rm Coil}}\frac{1}{r}dv-\frac{1+i_c}{4\pi}\cdot\frac{\mu_0\omega\sigma_i}{2}\sum_{e=1}^{NEJ}\delta_e\sum_{j=1}^{NBN}\times\left[\iint_{Se}\frac{\alpha_j(\xi,\eta)}{r}|\overrightarrow{A_1}\wedge\overrightarrow{A_2}|d\xi d\eta\right]\cdot\overrightarrow{J_{s,c,j}}. \tag{16}$$

At each node i of element J, the current density has two components, $J_{c,s,i1}$ and $J_{c,s,i2}$, and can be expressed by the following relation:

$$\overrightarrow{J_{c,s,i}}=J_{c,s,i1}\cdot\overrightarrow{t_{i1}}+J_{c,s,i2}\cdot\overrightarrow{t_{i2}} \tag{17}$$

where the vectors $\overrightarrow{t_{i1}}$ and $\overrightarrow{t_{i2}}$ are tangent to the surface of the current density element at node i. This two unit vectors are orthogonal and are calculated by taking the derivative of the polynomial functions.

The last step is the projection of Ohm's law onto these two vectors to obtain two linear relations on each node i.

When node i is an edge node, the density has only one component and only one projection is required. Therefore, in this special case, one relation is obtained for Ohm's law.

2) Conservation of the Current: The relationship $\mathrm{div}(\overrightarrow{J}) = 0$ is taken into account by integrating over a control volume. The following relation is obtained:

$$\mathrm{div}(\overrightarrow{J_c}) = 0 \quad \Leftrightarrow \quad \iiint_{\text{control volume}} \mathrm{div}(\overrightarrow{J_c}) dv = 0. \tag{18}$$

Using Green's theorem, we obtain

$$\int_{\Gamma} \overrightarrow{J_c} \cdot \overrightarrow{n_{\text{ext}}} d\gamma = 0 \tag{19}$$

where Γ is the boundary of the control volume and $\overrightarrow{n_{\text{ext}}}$ is the external normal to the control volume. In our case, the density current is tangent to the surface of the conductors and the control volume is the current density element. Consequently, this integral is the sum of the integrals on the edges of the current density element. We use a polynomial interpolation of the current density (11). On the edges of the element, the differential weight can be expressed by the vectors $\overrightarrow{A_1}$ and $\overrightarrow{A_2}$ defined in (15).

The density current at each node is expressed by the relationship (17), providing a second linear equation. The conservation of current is applied to each density current element. However, when the surface is closed, one relation is eliminated and replaced by a Dirichlet condition on V.

3) Linear System: This numerical formulation leads to a linear system

$$[M] * [U] = [K] \tag{20}$$

where $[M]$ is a full nonsymmetric matrix, $[U]$ is the vector of unknowns constituted by the components of the current densities and the electrical potential, and $[K]$ is the second vector of the system that is equal to the vector potential created by the coil when the current density is imposed in the coil. The terms $[M], [U], [K]$ are constituted by complex numbers. To solve this system, the Gauss method with a total pivot is used.

D. Particularities of the Method

The particularities of the method developed here are the same as those of the boundary-integral method.

- The matrix is full, nonsymmetric, and badly conditioned but the mesh is reduced to the surface of the conductors.
- A singular integral appears when node i is on the integration element. The numerical integration on this particular element is applied with a higher number of integration points. It is possible to test other numerical solutions.
- The magnetic induction is calculated by integration as in the boundary-element method. This gives more accurate results than the finite-element method.

E. Modeling the Symmetries and the Periodicity

To reduce the size of the linear system, we introduce the possibility of taking into account periodicity in the azimuth direction as well as planes of symmetry and antisymmetry. In this method, when a plane of symmetry or antisymmetry cuts a conductor, we impose a:

- Dirichlet condition on the electrical potential V on an antisymmetrical plane;
- Dirichlet condition on the normal component of the current density ($J_n = 0$) on a symmetrical plane.

However, in this method, the contribution of all the current densities to the magnetic vector potential must be taken into account. For this, new elements must be created using the symmetry, antisymmetry, or periodicity functions. Given that the integral must be taken over these new elements, the CPU time for the integral calculation of the terms of the matrix is not reduced as much as in other methods.

F. Values of Postprocessing

The unknowns of this method are the current density and the electrical scalar potential. Therefore, it is easy to calculate the following.

- The local values:
  - joule power density: $dP = (J \cdot J^*)/2\sigma$, where J^* is the conjugate of J;
  - magnetic induction $\overrightarrow{B}$ obtained using the Biot-Savart law;
  - electromagnetic force density $\overrightarrow{F} = \mathrm{Real}(\overrightarrow{J} \wedge \overrightarrow{B^*})/2$.
- The global values:
  - joule power in every conductor by integration of the power density;
  - electrical impedance $Z = R + i_c \omega L$, where R is the resistance and L is the inductance.

III. Numerical Results

To demonstrate the validity of this 3-D model, we have studied two different geometrical configurations. The results are compared with experimental measurements and the calculations obtained using quasi-3-D software developed a few years ago [14]. The latter is also based on an integral method, but was adapted to axisymmetric or cylindrical cold crucible configurations. This software is called axial software to differentiate it with respect to the new 3-D software.

A. Configuration no. 1

First, we study the simple problem consisting of a hexahedron-shaped load and an inductor with five turns. The configuration is illustrated in Fig. 5(a).

The height of the hexahedron is 0.1 m and its sides measure 0.06 m. It is made of copper ($\sigma = 5 \times 10^7\ \Omega^{-1} \cdot \mathrm{m}^{-1}$). The length of the sides of the square turns of the inductor is 0.08 m. The numerical simulation is carried out for a frequency of 20 kHz and a coil current of 1000 A. We analyze the results obtained for the global and local values.

1) Electrical Impedance Results: The influence of the mesh of the 3-D software package is studied on the equivalent elec-

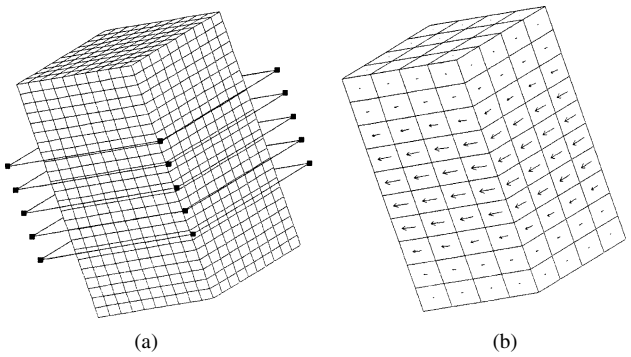

Fig. 5. Hexahedron load and inductor with five turns. (a) Geometry and mesh. (b) Current density vectors on the surface of the hexahedron.

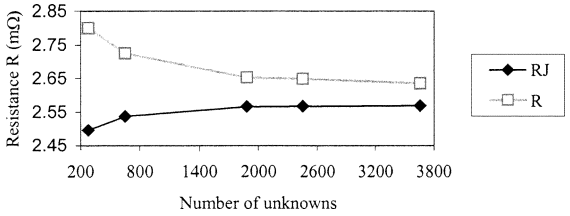

Fig. 6. Influence of the mesh on the value of the resistance.

TABLE I
INFLUENCE OF THE MESH ON THE VALUE OF THE INDUCTANCE

	Mesh 1	Mesh 2	Mesh 3	Mesh 4	Mesh 5
Unknowns	279	649	1849	2449	3657
L (μH)	- 0.899	- 0.908	- 0.924	-0.924	-0.927

TABLE II
ELECTRIC IMPEDANCE OBTAINED BY THE TWO SOFTWARE PACKAGES

	3D Software	Axial Software	Relative difference
R (mΩ)	2.635	2.28	15%
L (μH)	- 0.927	-0.933	0.6%

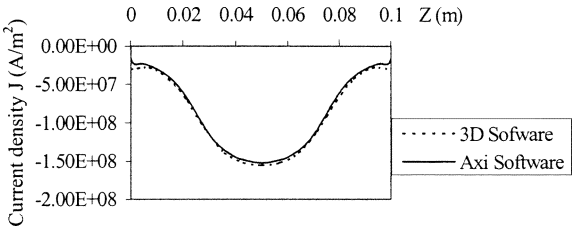

Fig. 7. Current density at 20 kHz on a vertical face of the hexahedron and cylinder. Hexahedron: 3-D software. Cylinder: axial software.

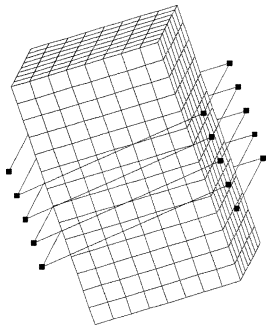

Fig. 8. Geometry and mesh of a hexahedron with a helical inductor.

trical impedance (Fig. 6 and Table I). The value of the resistance is obtained in two ways.

- The resistance R_J is deduced from the joule power in the load.
- The complex impedance is deduced from the vector potential calculated on the inductor. R and L represent the resistance and inductance of the load, respectively. The load is an electrical conductor, so this inductance value is negative (due to the eddy currents).

The two calculations of the resistance converge on asymptotic values for the refined mesh. The number of unknowns at convergence is about 3000. The resistance R_J converges faster than the resistance R. The difference between the two asymptotic values is around 2.5%. The dispersion of the values of inductance is rather small (Table I). The maximum error compared to the asymptotic value is 3%.

The results obtained by this 3-D software are compared with those obtained using the axial software (Table II). With the axial software, a cylindrical configuration designed to give the same induction flux was used.

There is very good concordance between the two numerical models for the inductance. For resistance, on the other hand, the relative difference between the two software packages is considerable (15%). However, the geometry of the two configurations is different: for the hexahedron, the load cross section is a square and for the cylinder, it is a circle. Given that the perimeter of the square is greater than that of the circle, it is normal that the resistance is greater for the hexahedron.

2) Current Density Results: This section presents the analysis of the distribution of the current densities. Fig. 5(b) shows the current density vectors on the surface of the hexahedron. The direction of the vectors is horizontal and they turn around the load. The higher densities are opposite the inductor.

A comparison between the current density distributions obtained by the two models, 3-D and axial, is presented (Fig. 7). The curves of the current density as a function of z are drawn. For the axial software, the component of the density is azimuthal. For the 3-D software, the curve is taken along a vertical line in the middle of a face (x, z) and the component of the density is on the x axis. The differences between the two curves are minor and are only noticeable at the extremities of the curves.

3) Helical Inductor: We will now look at the influence of the shape of the inductor. With the 3-D software, it is possible to study a helical inductor (Fig. 8).

The electrical impedance results obtained for the two configurations [Fig. 5(a) and Fig. 8] are compared in Table III. This 3-D effect has a significant influence on both the resistance and the inductance and affects the global values by 7% or 8%.

4) Conclusion: These results indicate that this 3-D software provides reliable values for global terms such as electrical impedance and local terms such as current density.

B. Configuration no. 2

We will now look at various 3-D cold crucible configurations (Fig. 9). These cold crucibles are made of copper $(\sigma = 5 \times 10^7\ \Omega^{-1} \cdot \mathrm{m}^{-1})$. The geometric characteristics of the cold crucible configurations are presented in Table IV.

To test this 3-D model, electrical impedance measurements were carried out. These measurements were based on the

TABLE III
INFLUENCE OF HELICITY ON THE IMPEDANCE (MESH 5)

	Configuration: Fig. 5	Configuration: Fig. 8	Difference
R (mΩ)	2.635	2.432	7%
L (μH)	-0.927	-0.850	8%

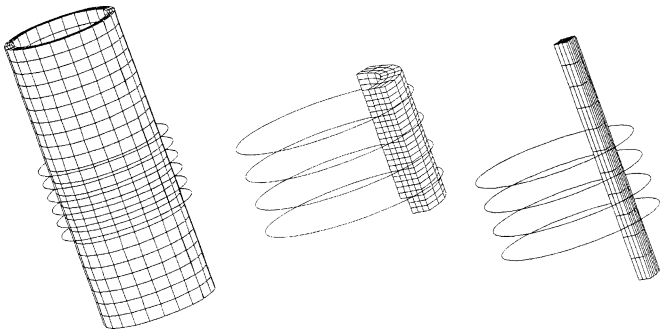

(a) (b) (c)

Fig. 9. Geometry and mesh of one segment of the three cold crucibles. (a) Cold crucible 1. (b) Cold crucible 2. (c) Cold crucible 3.

TABLE IV
GEOMETRICAL CHARACTERISTICS OF THE THREE COLD CRUCIBLE CONFIGURATIONS

	Crucible 1	Crucible 2	Crucible 3
Height	0.6m	0.06m	0.130m
External diameter	0.23m	0.08m	0.0654m
Internal diameter	0.22m	0.0605m	0.0495m
Number of slits	1	4	18
Slit width	0.8×10^{-3}m	0.8×10^{-3}m	0.7×10^{-3}m
Number of turns	6	4	4
Diameter of coil	0.27 m	0.084m	0.084m
Height of coil	0.14m	0.04m	0.04m

analysis of the electric discharge in an oscillating circuit. Tables V –VII present the impedance values and the percentage error of the model results with respect to measurements for the three cold crucibles.

The values of the electric impedance obtained using the 3-D software compare favorably with measurements. For crucibles 1 and 2, the relative error in the resistance determined by the 3-D model is relatively small (around 5%). On the other hand, the resistance determined by the axial software is far from the measured values for these crucibles. In the axial software, the periodicity of the cold crucible is taken into account but the segments are meshed into elementary currents with imposed directions. As a result, significant 3-D effects cannot be modeled. For the third crucible, both software packages provide results that compare well with the measured values, even if the 3-D method appears to be somewhat better. The two models have similar errors in inductance for crucible 1. The values of the inductance are better for the axial software package for crucibles 2 and 3. In the case of a cold crucible with a large number of segments, the 3-D software has no significant advantages over the axial software: the computing time is greater and the numerical results are no better.

For all of the examples considered, it appears that the 3-D software gives a good indication of the value of the impedance for a cold crucible configuration. Better results are obtained for the resistance than for the inductance.

TABLE V
IMPEDANCE OF COLD CRUCIBLE 1 AT 10 kHz

	Measurements	3D software		Axial Software	
Unknowns		4199	Error	2998	Error
R (mΩ)	5.56	5.274	5.1%	28.4	>100%
L (μH)	-3.17	-3.418	7.8%	-2.96	6.6%

TABLE VI
IMPEDANCE OF COLD CRUCIBLE 2 AT 25 kHz

	Measurements	3D Software		Axial Software	
Unknowns		1639	Error	748	Error
R (mΩ)	4.9	5.093	4%	6.48	32%
L (μH)	-0.426	-0.474	11.3%	-0.457	7.3%

TABLE VII
IMPEDANCE OF COLD CRUCIBLE 3 AT 25 kHz

	Measurements	3D software		Axial Software	
Unknowns		871	Error	998	Error
R (mΩ)	5.11	5.456	6.8%	4.232	17%
L (μH)	-0.229	-0.262	14.5%	-0.222	3%

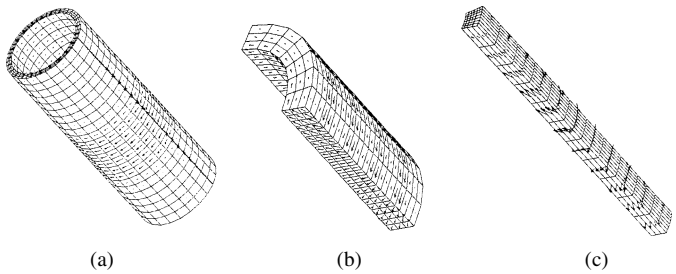

(a) (b) (c)

Fig. 10. Distribution of the current density on the surface of one segment of each cold crucible. (a) Cold crucible 1. (b) Cold crucible 2. (c) Cold crucible 3.

Fig. 10 shows the distribution of the current density at the surface of the three crucibles obtained by the 3-D software for a coil current of 1000 A.

The first cold crucible has only one slit and is higher than the inductor. On the external cylindrical face of the crucible, the current density is high in the middle, facing the inductor, and very low at the top and bottom. In the slit of the crucible, a significant vertical current density exists. For crucibles 2 and 3, the distribution of the current density on the external face is not uniform along the z axis. However, on the internal face, the distribution is quasi-uniform. Note that there is an important current density on the lateral face of the segment.

The distributions of the current density obtained by the two software packages are compared for the first cold crucible. Fig. 11 shows the variation of the azimuth component of the current density at the middle of the external cylindrical wall and Fig. 12 at the middle of the internal cylindrical wall. Fig. 13 and Fig. 14 present the curves of the two components (radial and vertical) at the middle of the lateral wall of the slit.

Fig. 11 and Fig. 13 show small differences between the current density curves obtained by the two models on the external and lateral walls. The horizontal component of the density has the same maximum facing the inductor. The most important difference appears on the internal wall of the cold crucible (Fig. 12). With the axial software, the horizontal current density shows a maximum opposite the inductor whereas with the 3-D software, the horizontal current is uniform along the z axis

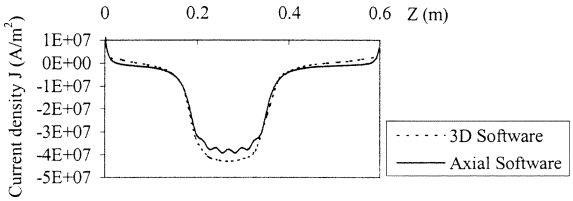

Fig. 11. Real part of the azimuth component of the current density on the external cylindrical wall.

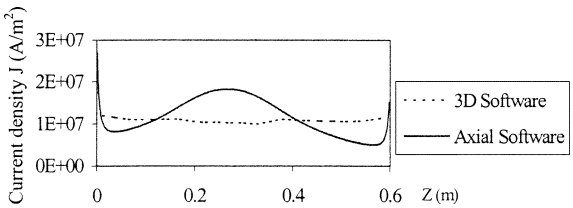

Fig. 12. Real part of the azimuth component of the current density on the internal cylindrical wall.

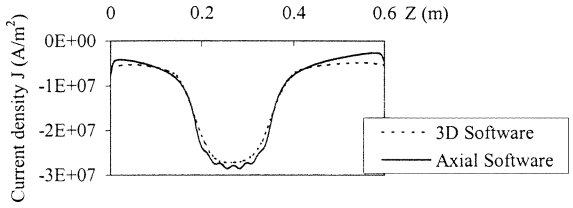

Fig. 13. Real part of the radial component of the current density on the lateral wall of the slit.

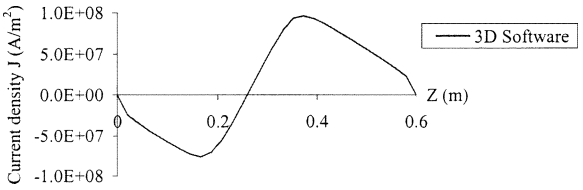

Fig. 14. Real part of the vertical current density on the lateral wall.

on the internal wall. This is due to the fact that the vertical component of the density is significant in the slit (Fig. 14). In the axial model, this effect cannot be modeled.

IV. Conclusion

This paper presents a new method, based on physical equations, for dealing with 3-D eddy-current problems. This method uses:

- an approach similar to the boundary element method for Ohm's law including a special solution involving numerical integration on 3-D surface elements;
- an approach similar to the finite-element method in terms of numerical derivation;
- the volume method for conservation of current.

In this way, we obtain a numerical model well-suited to induction problems in linear materials. This method is particularly effective for thin skin depths.

The validity of this method has been tested using examples. Numerical results for a hexahedron agree well with axial software results for an equivalent axial configuration. Numerical results for the electrical impedance using cold crucibles agree well with measurements. For cold crucibles, this software presents a significant advantage compared to the axial software when 3-D effects are significant, such as when the number of segments is small and the 3-D geometry must be taken into account.

Moreover, this approach can be used to study various geometrical configurations. The inductor coil can be easily modeled. In this way it is now possible, for example, to study the effect of inductor coil helicity and the influence of the connections.

References

[1] O. Biro and K. Preis, "On the use of the magnetic vector potential in the finite-element analysis of three-dimensional eddy currents," *IEEE Trans. Magn.*, vol. 25, pp. 3145–3159, July 1989.

[2] Y. Kawase and T. Yoshida, "3-D finite element analysis of molten metal shape in rectangular cold crucible system," *IEEE Trans. Magn.*, vol. 35, pp. 1889–1892, May 1999.

[3] D. Albertz and G. Henneberger, "Calculation of 3D eddy current using both electric and magnetic vector potential in conducting regions," *IEEE Trans. Magn.*, vol. 34, pp. 2644–2647, Sept. 1998.

[4] H. Tsuboi, M. Tanaka, T. Misaki, and T. Naito, "Three-dimensional analysis of eddy current and electromagnetic force in cold crucibles," *IEEE Trans. Magn.*, vol. 30, pp. 3499–3502, Sept. 1994.

[5] H. Tsuboi, M. Tanaka, F. Kobayashi, and T. Misaki, "Three-dimensional eddy current analysis of induction melting in cold crucibles," *IEEE Trans. Magn.*, vol. 29, pp. 1574–1577, Mar. 1993.

[6] N. Aymard, M. Feliachi, and B. Paya, "An improved modified surface impedance for transverse electric problems," *IEEE Trans. Magn.*, vol. 33, pp. 1267–1270, Mar. 1997.

[7] S. Yuferev and L. Kettunen, "Implementation of high order surface impedance boundary conditions using vector approximating functions," *IEEE Trans. Magn.*, vol. 36, pp. 1606–1609, July 2000.

[8] S. Yuferev and N. Ida, "Selection of the surface impedance boundary conditions for a given problem," *IEEE Trans. Magn.*, vol. 35, pp. 1486–1489, May 1999.

[9] F. Z. Louai, D. Benzerga, M. Feliachi, and F. Bouillault, "A 3D finite element analysis coupled to the impedance boundary condition for the magnetodynamic problem in radiofrequency plasma devices," *IEEE Trans. Magn.*, vol. 32, pp. 812–815, May 1996.

[10] B. Dumont and A. Gagnoud, "3D finite element method with impedance boundary condition for the modeling of molten metal shape in electromagnetic casting," *IEEE Trans. Magn.*, vol. 36, pp. 1329–1332, July 2000.

[11] J. Shen, Z. Andjelic, and B. Schaub, "A hybrid single and dual simple layer boundary integral equation formulation for 3-D eddy currents," *IEEE Trans. Magn.*, vol. 34, pp. 2636–2639, Sept. 1998.

[12] L. Krahenbuhl, O. Fabregue, S. Wanser, M. De-Sousa-Dias, and A. Nicolas, "Surface impedances, BIEM and FEM coupled with 1D nonlinear solutions to solve 3D high frequency eddy current problems," *IEEE Trans. Magn.*, vol. 33, pp. 1167–1172, Mar. 1997.

[13] B. Maouche and M. Feliachi, "Analysis of the eddy current effect on the impedance of an electromagnetic system supplied by LF or HF voltage and using a discretized integral method," *J. Physique-III*, vol. 7, pp. 1967–1973, Oct. 1997.

[14] A. Gagnoud and I. Leclercq, "Electromagnetic modeling of induction melting devices in cold crucibles," *IEEE Trans. Magn.*, vol. 24, pp. 573–575, Jan. 1988.